Available online at www.sciencedirect.com
SCIENCE DIRECT
Global and Planetary Change 52 (2006) 71–87
GLOBAL AND PLANETARY CHANGE
www.elsevier.com/locate/gloplacha

An integrated dust storm prediction system suitable for east Asia and its simulation results

Jianhua Sun [a,*], Linna Zhao [b], Sixiong Zhao [a], Renjian Zhang [c]

[a] *Laboratory of Cloud Physics and Severe Storms, Institute of Atmospheric Physics, Chinese Academy of Sciences, Beijing 100029, China*
[b] *National Meteorological Center, China Meteorological Administration, Beijing 100081, China*
[c] *Key Laboratory of Regional Climate-Environment Research for Temperate East Asia (REC-TEA), Institute of Atmospheric Physics, Chinese Academy of Sciences; START Regional Center for Temperate East Asia, Beijing 100029, China*

Accepted 9 February 2006
Available online 21 April 2006

Abstract

An integrated dust storm modeling system is developed for the prediction of dust storms. The system couples a wind erosion scheme, a dust transportation model and the Penn State/UCAR modeling system (MM5) with a geographic information database. The system can be used for the prediction of dust emission rate and dust concentration associated with individual dust storm events. Two severe dust storm events occurred in spring 2002, one on the 19th–22nd of March and the other on the 6th–9th of April. The integrated modeling system is used to simulate the two events. The numerical results are compared with surface weather records and satellite images and good agreement is found between the model results and observation in dust concentration distribution and evolutions. The Gobi Desert in southern Mongolia and the Badain Jaran Desert, Tengger Desert and Hunshandake sandy land in Inner Mongolia (China) are identified to be the dust sources for the two events. The dominant modes of dust particles over western Inner Mongolia and Mongolia are from 2 to 11 μm in size, and 2 to 22 μm over Beijing and its surrounding area. The emission of particles in the 2–11 μm size range is found to be most important for Northeast Asian dust storms.

Keywords: dust storm; wind erosion; dust transportation; GIS data

1. Introduction

Dust storms frequently occur in Northeast Asia, especially in spring when strong winds entrain large quantities of dust particles into the atmosphere and carry them downstream (Zhang, 2001). Extremely severe dust storms in the past have resulted in the loss of human lives and the disruption of economic activities (Cheng and Ma, 1996). According to the synoptic records over the past 50 yr or so, 2000, 2001 and 2002 are active years of severe dust storm (Zhang et al., 2002). While dust storms are widely recognized as a serious environmental problem in China and have attracted much scientific attention, the main research carried out within China so far has been mainly on the synoptic and climatic features of dust storms (e.g. Ye et al., 2000; Zhou, 2001), rather than on their numerical modeling and prediction.

Quantitative dust storm prediction is not possible unless dust emission, transportation and deposition

* Corresponding author. P.O. Box 9804, Beijing, 100029, PR China. Tel.: +86 10 82023312.
E-mail address: sjh@mail.iap.ac.cn (J.H. Sun).

0921-8181/$ - see front matter © 2006 Elsevier B.V. All rights reserved.
doi:10.1016/j.gloplacha.2006.02.005

involved in the dust cycle are all correctly simulated. The simulation of dust sources is the first key question to be addressed (Shao, 2000). However, dust emission involves complex physical processes that are not yet well understood. Its study requires the knowledge of atmospheric sciences, fluid dynamics, soil physics, surface hydrology, etc. Although numerous studies in China have been carried out on dust transportation (Liu and Cheng, 1997; Liu et al., 1998; Huang and Wang, 1998; Li et al., 1998), quantitative simulation of dust emission has rarely been done in China until recently. However, in most previous studies, the crude dust source parameterization schemes used do not meet the requirements of dust storm prediction (Liu et al., 1998; Wang et al., 2000). Some significant progresses have been made in the past two decades (for a review see Raupach and Lu, 2004). In particular, better wind erosion schemes have been developed which account for the impact of surface properties on dust emission (Marticorena and Bergametti, 1995; Shao et al., 1996; Marticorena et al., 1997; Shao, 2001, 2004). For example, Lu and Shao (2001) have applied such a scheme for the prediction of dust storms in Australia with much success. Chemical process has also been considered in some dust entrainment and deposition models (Zender et al., 2003).

The aim of our study is to develop an integrated modeling system to be used for the operational prediction of dust storms in East Asia. As the occurrence of East Asian dust storm is closely associated with severe weather systems, we select a non-hydrostatic meso-scale atmospheric model for the integrated modeling system. In our study, the Penn State/NCAR (National Center for Atmospheric Research) MM5 modeling system (Grell et al., 1994) is used. The dust emission scheme of Shao (2001, 2004) is used for the simulation of dust sources. The dust emission scheme and a dust transportation scheme, together with a GIS database are then integrated into MM5 and applied to simulating dust storms in northern China. A brief description of the coupled system is presented in Section 2. The severe dust storms in spring 2002 and the weather patterns of the two dust storm episodes are described in Section 3. Simulation results are verified with observations, and dust sources are analyzed in Section 4. Finally, conclusions and discussions are given in Section 5.

2. The integrated numerical modeling system

2.1. The integration of the modeling system

The structure of our system is illustrated in Fig. 1. It consists of a GIS database, a pre-processor for the dust emission model, a limited regional weather model (MM5V3 together with a land surface model), a dust emission model and a dust transportation model. The weather, dust emission and dust transportation models in the dashed frames in Fig. 1 are coupled together and are integrated at every time step. The dust emission model is coupled with the NCEP MRF (National Center for Environmental Prediction, Medium-Range Forecast model) high resolution PBL (Planetary Boundary Layer) scheme (Hong and Pan, 1996) and OSU/Eta (Oregon State University Eta model) land surface model (Chen and Dudhia, 2001a, b). The atmospheric model provides atmospheric data to force the wind erosion and dust transportation models. For each time step, the friction velocity from the PBL scheme and the surface soil moisture from the land surface scheme are passed to the wind erosion model for the calculation of the dust emission rate for different particle size groups. The dust emission rate and atmospheric variables (temperature, horizontal wind, vertical velocity, etc.) are then passed to the dust transportation model for computing instantaneous grid-mean dust concentration. The parameters of soil and vegetation states, required by the dust emission scheme, are prepared by a GIS pre-processor. What follows is the brief introduction of the MM5 modeling system, wind erosion and dust transportation models.

2.2. The MM5 modeling system

The fifth-generation Mesoscale Model (MM5), jointly developed by The Pennsylvania State University (Penn State) and the National Center for Atmospheric Research (NCAR), is a meso-scale modeling system that includes a multiple-nest capability, non-hydrostatic dynamics and a four-dimensional data assimilation capability as well as various physics options (Grell et al., 1994). This meso-scale model is widely used for numerical weather prediction.

The left panel in Fig. 1 is the MM5 flow chart. Terrestrial and land-use data are ingested and interpolated to the grids of model domain by programs TERRAIN on either a Mercator, Lambert Conformal or Polar Stereographic projection. Isobaric meteorological data are horizontally interpolated by programs REGRID from a latitude–longitude mesh to the grid of a model domain. Since the interpolation does not provide meso-scale detail, the interpolated data may be enhanced (program RAWINS/Little_r) with observations from the standard network of surface and rawinsonde stations. Finally, the program INTERP performs the

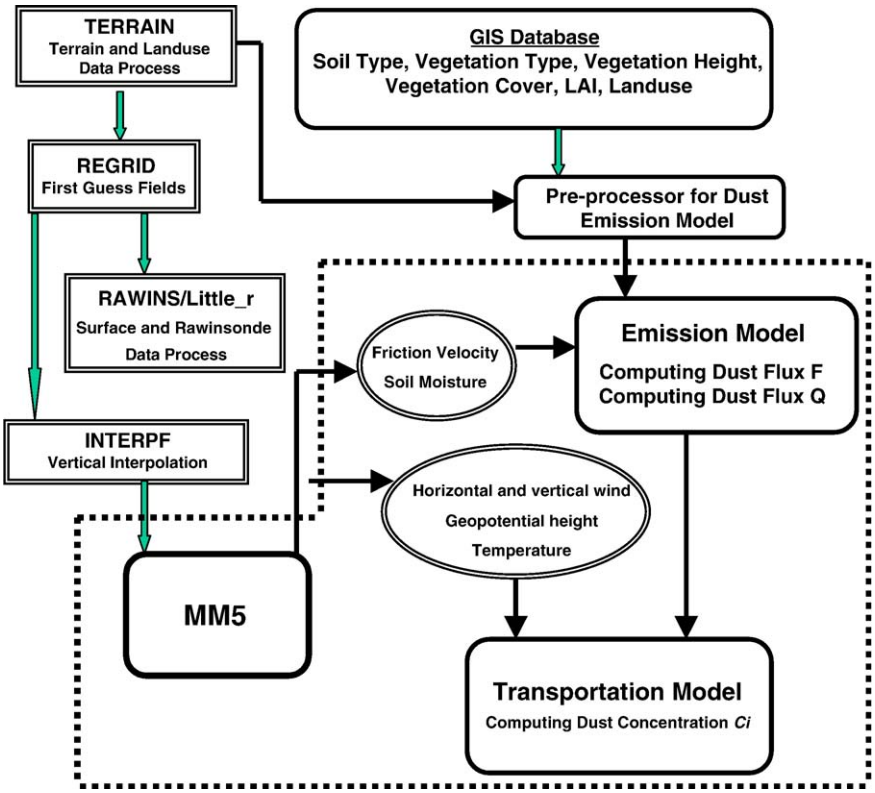

Fig. 1. The framework of the integrated dust storm modeling system.

vertical interpolation from pressure levels to the sigma coordinate system of MM5.

The land surface model in MM5 is a special scheme which relates to the simulation of dust emission. This OSULSM (Oregon State University Land Surface Model) was implemented in the NCEP operational Eta Model in February 1996. The coupled Eta-OSULSM system indeed improves the short-range prediction of the surface heat fluxes, near-surface sensible variables, boundary layer and precipitation, therefore OSULSM is also used in MM5 (Chen and Dudhia, 2001a,b). OSULSM has one canopy layer and calculates a number of prognostic variables, including soil moisture and temperature in the soil layers, water stored in the canopy, and snow stored on the ground. The model has four soil layers, and the thickness of each layer from the ground surface to the bottom is 0.1, 0.3, 0.6, and 1.0 m, respectively.

2.3. Dust emission scheme in wind erosion model

In this study, the dust emission scheme proposed by Shao (2001) is used to calculate the dust emission rate. The details of the scheme can be found in the latter paper (see also Shao, 2004 for a simplification). Here, the computation of some key variables (threshold friction velocity, streamwise sand flux, dust emission flux, etc.) will be briefly introduced. In the dust emission scheme, whether or not the dust emission rate is calculated depends on the friction velocity (u_*) and threshold friction velocity (u_{*t}). Dust emission will only be computed when u_* is greater than u_{*t}. The latter quantity is calculated using the following expression (Shao and Lu, 2000):

$$u_{*_t} = RHMu_{*t0} = RHM\sqrt{a_1\left(\sigma_p g d + \frac{a_2}{\rho d}\right)} \qquad (2.1)$$

where u_{*t} is the threshold friction velocity for uniform particles over a bare, dry and loose soil surface, d is the particle diameter, g is acceleration due to gravity, ρ is the density of air and σ_p is the particle-to-air density ratio. The coefficients a_1 and a_2 ($a_1=0.0123$ and $a_2=3\times10^{-4}$ kg s^{-2}) are determined by fitting u_{*t0} to wind tunnel datasets. R, H and M represent the influences of surface roughness elements, soil moisture and soil aggregation, respectively, which can be

calculated using soil and vegetation parameters from the GIS database.

Previous studies indicate that dust emission is mainly due to the saltation of soil particles (Shao, 2000). For each particle size group, the dust emission model calculates saltation sand flux Q_i (mg m^{-1} s^{-1}) and vertical dust flux F_i (mg m^{-2} s^{-1}). Q_i are calculated according to the following equation:

$$Q_i(d) = \begin{cases} (c\rho u_*^3/g)[1-\mu_{*_t}(d)/u_*][1+(u_{*t}(d)/u_*)^2] & u_* \geq u_{*_t} \\ 0 & u_* < u_{*_t} \end{cases} \quad (2.2)$$

where c is an empirical coefficient equal to 2.6. The contribution to the total flux of each size range is assumed to be proportional to its weight fraction in the soil particle size distribution. The total saltation sand flux is then evaluated as a weighted integral of $Q_i(d)$ over all particle sizes, i.e.:

$$Q = \int Q_i(d)p(d)\delta d \quad (2.3)$$

where $p(d)$ is particle size distribution. To take the effects of non-erodible elements into consideration, saltation sand flux is multiplied by two factors: $Q_m = Q \times E_s \times E_v$. Here, E_v and E_s represent the surface area friction covered by vegetation and other roughness elements, respectively.

The vertical dust flux is expressed as (Lu and Shao, 1999):

$$F(d) = \frac{C_\alpha g f \rho_b}{2p}\left(0.24 + C_\beta u* \sqrt{\frac{\rho_p}{p}}\right)Q \quad (2.4)$$

where f is the total volumetric fraction of dust in the sediment, ρ_b is the bulk soil density, ρ_p is the particle density, p is the soil plastic pressure exerted by the soil on a particle impacting on it, for most natural soils, is larger than 10^5 N m^{-2}, and C_α and C_β are coefficients of order 1. An integration of Eq. (2.4) over the sand particle-size range gives the total vertical dust flux from the surface.

Most airborne dust particles are in the size range of 1–10 μm, although particles of up to 60 μm are observed during severe dust events (Zhuang et al., 2001). In this study, six particle size groups are considered: $d \leq 2$ μm (clay), $2 < d \leq 11$ μm (fine silt), $11 < d \leq 22$ μm (medium silt), $22 < d \leq 52$ μm (large silt), $52 < d \leq 90$ μm (fine sand), and $90 < d \leq 125$ μm (medium sand). In addition, the dust emission scheme requires minimally and fully dispersed particle size distributions [$p_m(d)$ and $p_f(d)$], which can be obtained by analyzing samples of parent soil. A quality data set of $p_m(d)$ and $p_f(d)$ is not available for Asia. In the present study, $p_m(d)$ and $p_f(d)$ are reconstructed as a composite of several lognormal distributions (Chatenet et al., 1996).

The land surface parameters required by the dust emission model include soil type, land-use index, vegetation type, vegetation height, leaf area index (LAI) and vegetation cover. The soil type and vegetation type for regions outside and inside of China are obtained from EOSDIS (Earth Observing System Data and Information System), FAO/UNESCO (Food and Agriculture Organization/United Nations Educational, Science and Cultural Organization) data and 1:4,000,000 Chinese soil data, respectively. Soil type data for China is provided by LREIS (State Key Laboratory of Resources and Environment information System, Chinese Academy of Sciences) data. Soil in China is classified into more than 50 primary types and a reclassification of the data into the USDA (United States Department of Agriculture) soil texture classes is made by examining its classification (Zhang et al., 2004). The LREIS, EOSDIS and FAO/UNESCO data are merged to build a vegetation and soil data set for the simulation. There are 12 USDA soil texture classes and 17 IGBP (International Geosphere-Biosphere Programme) vegetation types. Other parameters, such as leaf area index (LAI), are retrieved from remote sensing data. The resolution of all parameters are $3' \times 3'$.

The resolution of GIS data is much higher than that of the atmospheric model. Therefore, a pre-processor for the dust emission model is designed to interpolate the fine resolution GIS data onto the atmospheric model grid. To increase the accuracy in the calculation of dust emission, the mosaic subgrid closure is used (Lu and Shao, 2001), which can minimize the information loss of the original land surface data and at the same time allows for computational efficiency. In the pre-processor, on the basis of GIS data, the surface is classified into water, non-erodible and erodible lands, and dust emission is computed only for erodible lands. Each model grid is divided into several fractions according to the soil type, and the subgrids of the same soil type are put together regardless of their location in the model grid.

2.4. Dust transportation model

Dust particles are classified into six size groups. Advection, diffusion and dry deposition are considered the transportation model. The transportation model domain and grid are the same as the MM5 model. Meteorological variables obtained from MM5 are fed to

the transportation model at every time step. The wet removal process and the chemical processes are not considered in this study.

3. The severe dust storm events in the spring of 2002

Dust events are classified into four categories: dust-in-suspension, blowing dust, dust storm and severe dust storm according to the criterion of WMO GTS (World Meteorological Organization, Global Telecommunication System) code. The definitions of these classes are made according to horizontal visibility. The horizontal visibility of dust-in-suspension, blowing dust, dust storm and severe dust storm are less than 10 km (under moderate wind conditions), 1 to 10 km (under strong wind conditions), 500 to 1000 m and less than 500 m, respectively. To this day, traditional weather records obtained from the routine meteorological networks are the best data to analyze the features of dust storm activities. In this section, three-hourly routine surface observations in the spring of 2002 are used to analyze the features of dust storm activities.

The number of dust events is used to study the dust-affected area and intensity, although the distribution of the stations is not well-proportioned, especially in northwestern China and Mongolia. The analysis region is defined by 30–60°N and 90–140°E, which includes the northern part of China, Mongolia, the Korean peninsula and Japan. All dust events are divided into

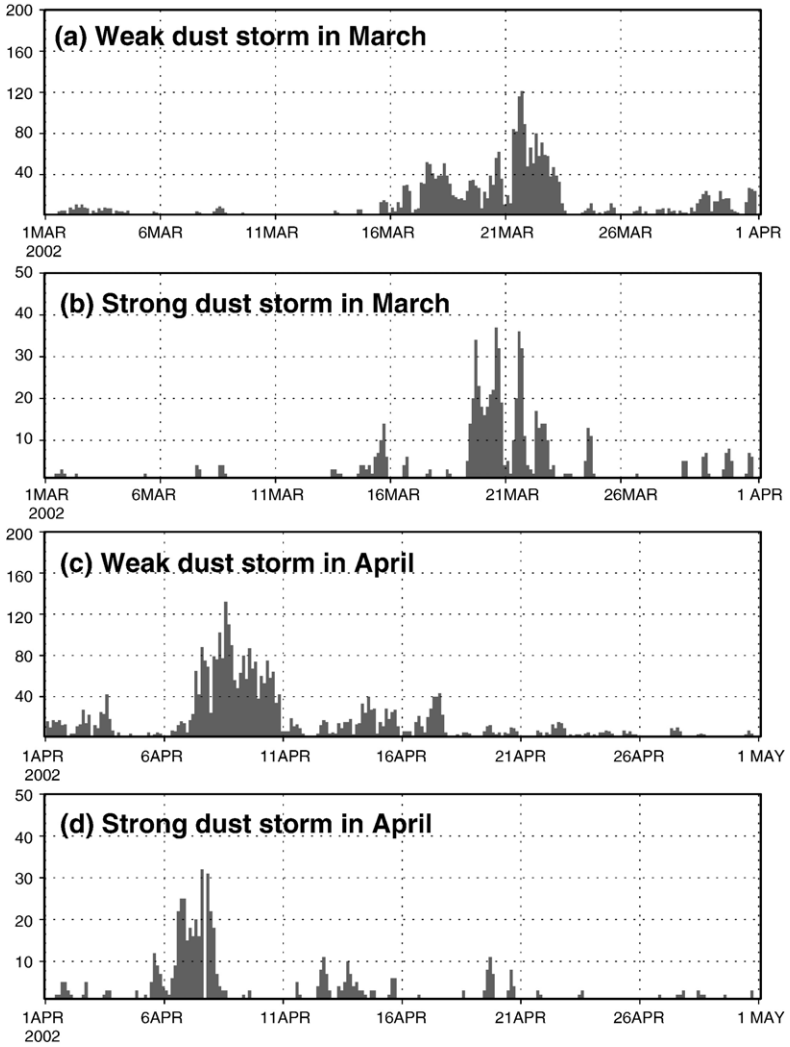

Fig. 2. The number of stations at which the weak dust storm and strong dust storm are recorded in the region of 30–60°N and 90–140°E in March and April 2002.

two categories: weak dust events including dust-in-suspension and blowing dust, and strong dust events including dust storm and severe dust storm. Since no severe dust events were recorded in May 2002, Fig. 2 only shows the total numbers of weak dust storms and strong dust storms in March and April 2002. As can be seen, dust events occurred continuously during March 15–25 and April 5–18 over the areas of 30–60°N and 90–140°E (Fig. 2a, c). Less dust events occurred in April in comparison to March. Observations show that two severe dust storms occurred on March 19–22 and April 6–9 (Fig. 2b, d). Both events lasted more than three days with more than 30 stations recording dust storms at one time.

Obvious diurnal variation occurred in dust storm intensity. To illustrate the diurnal variation, the number of stations for four categories of dust events at 0200, 0500, 0800, 1100, 1400, 1700, 2000, and 2300 LST (LST = UTC + 8 h,) in one day are displayed in Fig. 3. Dust-in-suspension events appear more frequently in the morning or at noon (0800 or 1400 LST), while severe dust storms often occur in the afternoon (1400 or 1700 LST). The diurnal variation of severe dust storm is stronger than that of light dust storm. This is probably due to the fact that the Planetary Boundary Layer (PBL) is most unstable during the afternoon. All of the four categories of dust events are relatively weak from 23 LST to 05 LST. The PBL related to daily variation of dust events should be investigated in future.

The 19th–22nd of March and the 6th–9th of April dust events will be investigated in detail in this study. The weather patterns of the two events will be described first, and then the integrated modeling system will be

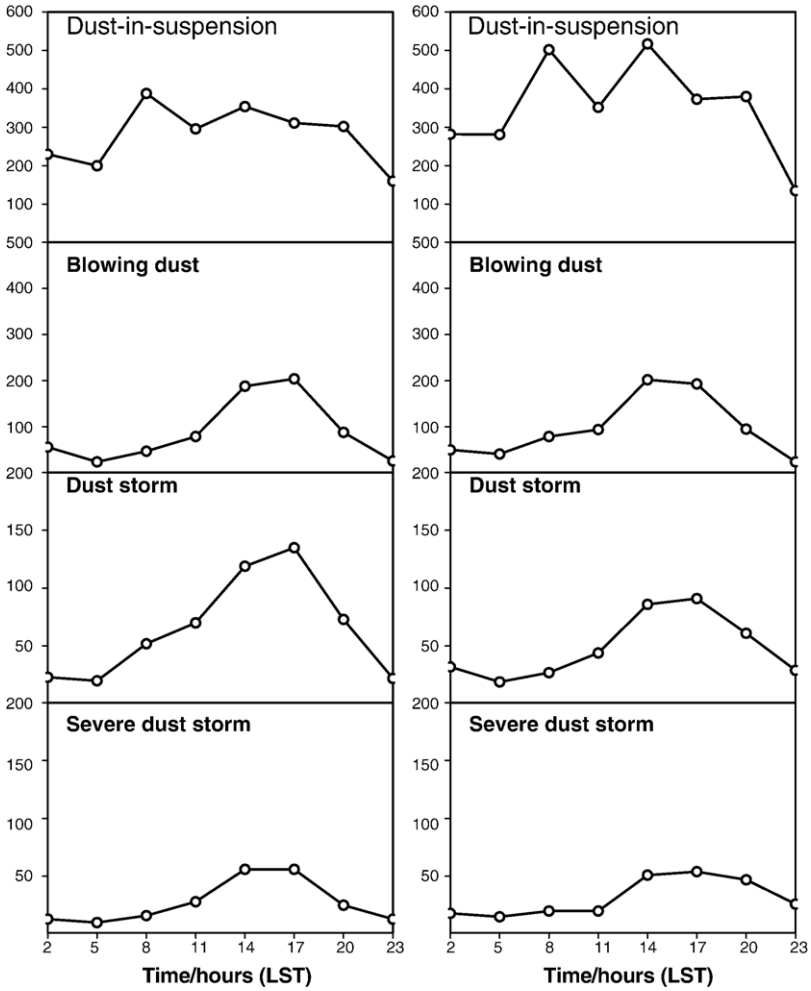

Fig. 3. Daily variation of the number of stations at which dust-in-suspension, blowing dust, dust storm, and severe dust storm are recorded in March (left panel) and April (right panel) 2002.

employed to simulate the development of the weather system, dust emission and transportation.

Dust storms in northeastern Asia occur mostly under the strong cold air flows associated with Mongolian cyclones. The affected areas are somewhat different as the cyclones propagate eastwards along different paths. North China, the Korean Peninsula and Japan are affected seriously if the cyclone travels the southern pathway, otherwise northeastern China is more affected. Both the 19th–22nd of March and the 6th–9th of April 2002 storms were produced by Mongolian cyclones. Fig. 4 shows the geopotential height and temperature at 500 hPa for the two cases. A deep trough was moving eastwards from 90°E at 0000 UTC March 19 to the eastern coastal region at 0000 UTC March 22 (Fig. 4a–d). In the early stages, the trough traveled very fast, moving from eastern Xinjiang (at 0000 UTC March 19) to east Mongolia in 24 h, at a speed of about 2000 km/day. In the later stages, the trough propagated relatively slowly. At the ground surface, a cyclone formed over central Mongolia at 0000 UTC March 19 (not shown). Very strong northwesterly wind with a maximum velocity exceeding 20 m s^{-1}, behind the surface cold front, resulted in blowing dust and dust storm over southern Mongolia (not shown). With the propagation of the trough aloft, the cyclone moved to eastern Mongolia and northeastern Inner Mongolia, and dust storm to severe dust storm weather occurred in Inner Mongolia, northeastern China and the Korean Peninsula.

The 6th–9th of April 2002 event was also produced by a Mongolian cyclone in the lower troposphere and a deep trough or a cut-off low aloft (Fig. 4e–h). The propagation path of this cyclone is almost the same as the previous event except it is shifted slightly northeastward. Therefore, the first event affected a wide area with dust invading 35°N, while the second event affected a relatively narrow area with dust invading 40°N (not shown).

During the period of spring, Mongolian cyclones often form and develop over Mongolia and Inner Mongolia. The mechanism of their formation and development has been investigated by Zhao and Zhao (2006-this issue). It is found that cold advection and baroclinic forcing are favorable to the rapid development of the cyclone. The interaction between upper and lower level systems is obvious during the development of the cyclone, and this can be confirmed by strong updraft and a deep sink of the tropopause. In the present study, we focus on the simulation of dust storms, instead of the Mongolian cyclones and their mechanism in details.

4. Validation and analyses of the simulation results

In this section, we first verify the simulation results using synoptic records and satellite images and then examine the dust sources for the two events.

4.1. Model configuration and initiation

The simulation domain covers an area which contains Mongolia, China, the Korean Peninsula and Japan, centered at 45°N and 110°E. The area has 142×163 grid points with a horizontal resolution of 45 km. The model top is located at 100 hPa and has 24 vertical sigma levels.

Six-hourly global analyses data, with a $1° \times 1°$ resolution from the NCEP, USA, are interpolated horizontally onto the model grid points. Then, they are interpolated from pressure levels onto the model σ levels. The dust concentration of each particle size group is given as zero initially. The numerical integrations start at 0000 UTC March 19 and 0000 UTC April 6 2002, respectively, and end at 0000 UTC March 22 and 0000 UTC April 9 2002, respectively. The time-dependent, lateral boundary conditions are provided by interpolating the six-hourly observational analyses linearly in time. Indeed, the soil moisture is a very important component of land surface modeling, and it would not make much sense to implement a sophisticated Land Surface Model (LSM) in meso-scale models without a proper soil moisture initialization procedure. However, there are no routine soil moisture observations. Thus, the initialization of the LSM will largely depend on soil moisture fields obtained from analysis/forecasts from other models. In the current model, the initial soil moisture can be obtained from the NCEP reanalysis system because a similar LSM is used in this system and the soil moisture fields are compatible to the MM5-LSM. The reanalysis volumetric soil moisture fields for two soil layers, 0–10 and 10–200 cm, are interpolated to the four soil layers in the MM5-LSM.

4.2. Validation with synoptic data and satellite images

4.2.1. Dust event during the 19th–22nd of March 2002—case one

In Fig. 5, the simulated dust concentration and observational surface weather phenomena are compared at 0300 and 0600 UTC of the 19th, 20th, and 21st of March. This figure shows that the spatial distribution and temporal evolution of the simulated and observed dust storm are in general agreement. The dust storm first developed on March 19 in the Gobi desert over southern

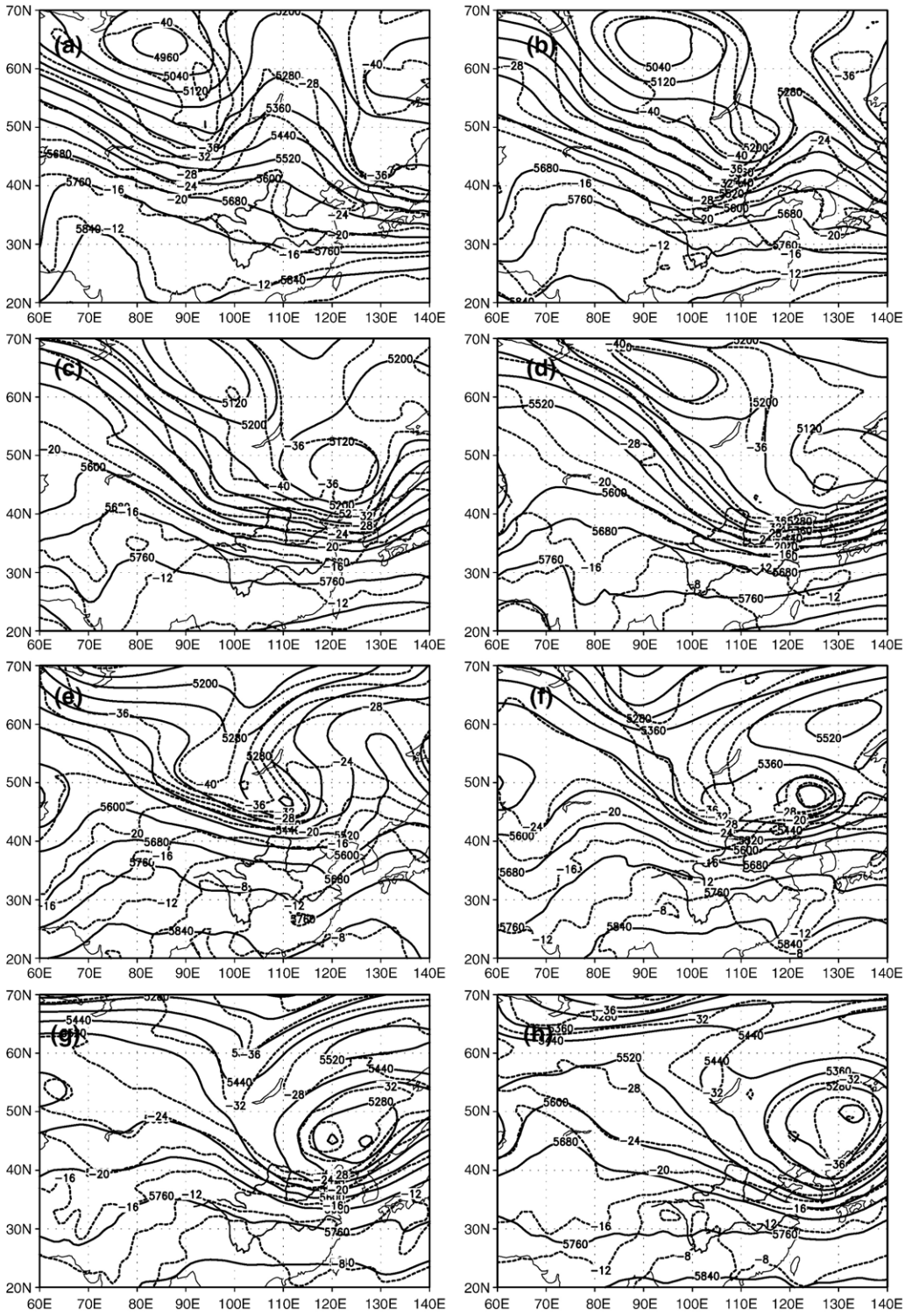

Fig. 4. Geopotential height (solid line, units: gpm) and temperature (dashed line, units: °C) on 500 hPa at (a) 0000 UTC March 19; (b) 0000 UTC March 20; (c) 0000 UTC March 21; (d) 0000 UTC March 22; (e) 0000 UTC April 6; (f) 0000 UTC April 7; (g) 0000 UTC April 8; and (h) 0000 UTC April 9, 2002.

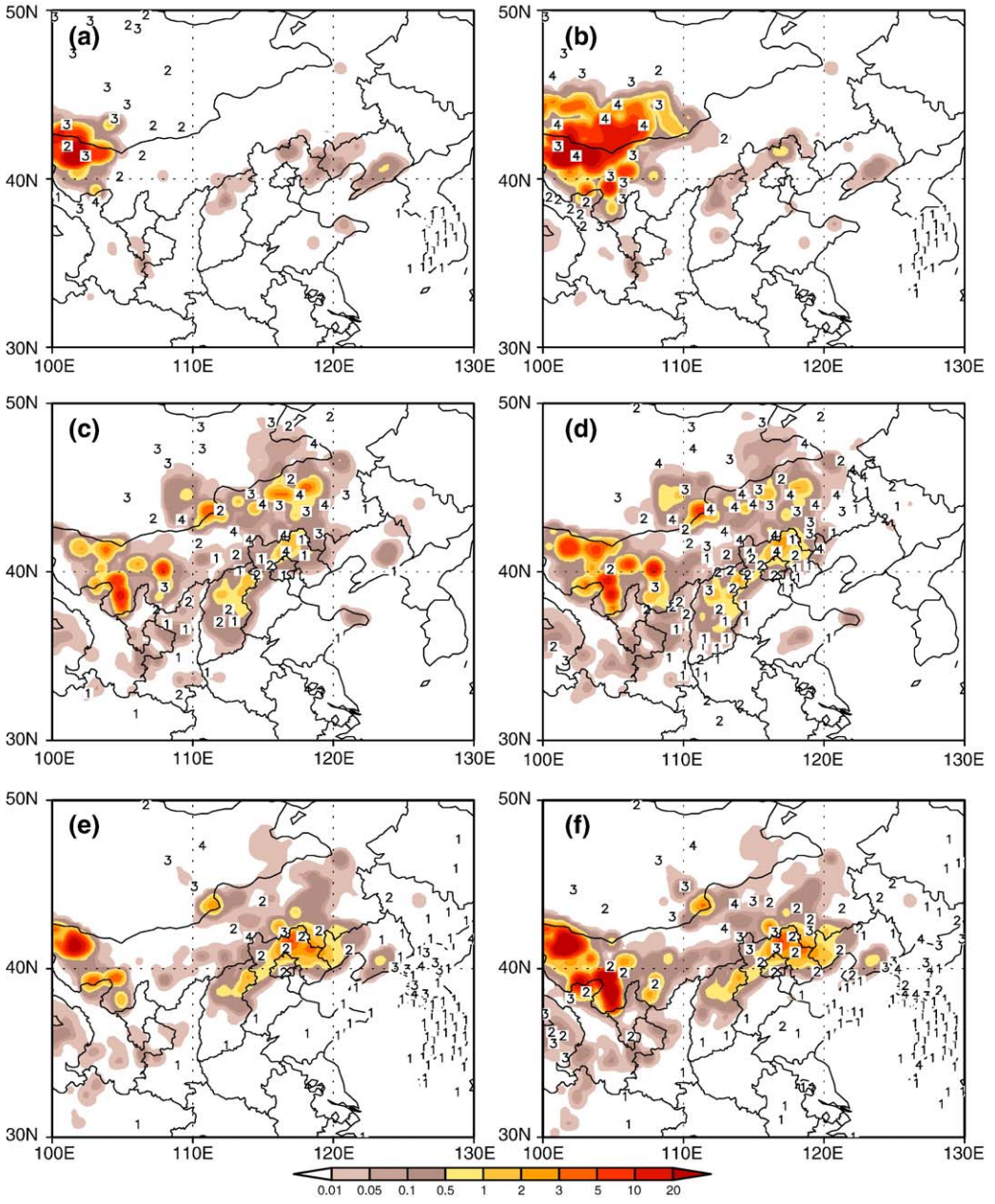

Fig. 5. A comparison of simulated surface dust concentration (shaded, units: mg m^{-3}) and observed surface weather phenomena (1, 2, 3 and 4 representing dust-in-suspension, blowing dust, dust storm and severe dust storms, respectively). (a) 0300 UTC March 19; (b) 0600 UTC March 19; (c) 0300 UTC March 20; (d) 0600 UTC March 20; (e) 0300 UTC March 21; and (f) 0600 UTC March 21, 2002.

Mongolia and the Alashan Plateau, Tengger Desert in Inner Mongolia (Fig. 5a, b). The simulated dust concentration in the (severe) dust storm recorded regions is greater than 10 mg m^{-3}. On the next day (March 20), the dust storm moved eastwards, spreading widely and affecting most of Inner Mongolia, Shanxi and Hebei provinces and a severe dust storm occurred in the vicinity of the Hunshandake sandy land (Fig. 5c, d). Both the simulation and observation show that a 2000-km long dust band extended from northeastern China to the north of the Yangtze River. The dust storm on March 21 was weaker than on March 20, and the dust-affected area was reduced to Beijing, northern Hebei province and in the neighborhood of the Hunshandake sandy land (Fig. 5e, f). From the evolution of the dust event, the

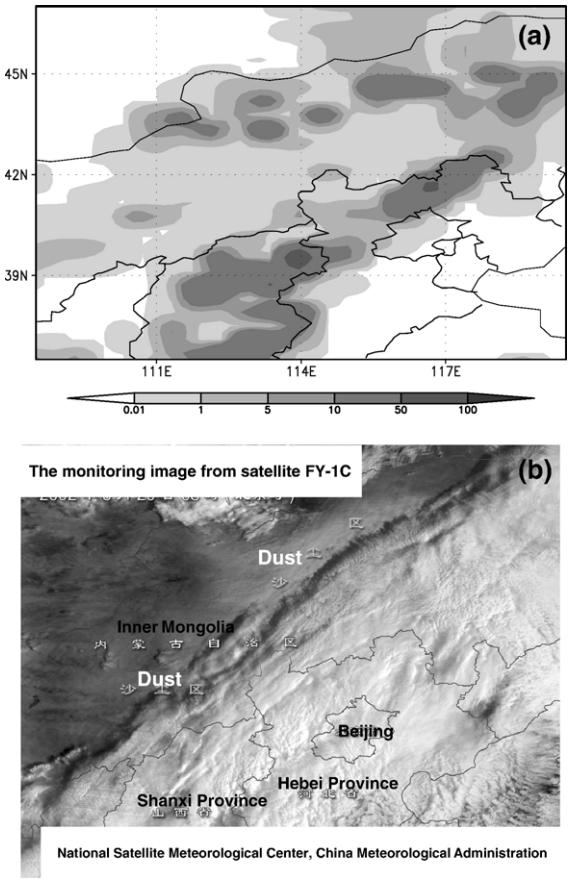

Fig. 6. (a) Simulated dust concentration in mg m^{-2} integrated vertically from surface to model top layer, and (b) satellite images from FY-1C for 0000 UTC March 20, 2002.

main dust source place of this event is the Gobi desert in Mongolia and the sandy lands in the western part of Inner Mongolia.

A comparison of satellite image and simulated dust concentration integrated from the surface to the model top layer at 0000 UTC March 20 is given in Fig. 6. The simulated dust-affected region over Inner Mongolia agrees well with the observation, but the simulated dust regions over Shanxi and Hebei provinces, covered by cloud, cannot be found in the satellite image. However, the observed weather phenomena at 0000 UTC March 20 (not shown) reveal that the dust storm was approaching to Shanxi and Hebei provinces.

The dust events in spring 2002 were monitored by the scientists at the Institute of Atmospheric Physics, Chinese Academy of Sciences (IAP/CAS) in Beijing (Zhang et al., 2005), and the monitoring site was located at 39°58′N, 116°22′E. A high-volume air sampler HV-1000F (SIBATA Scientific Co., Japan) was used to collect total suspended particle (TSP) samples. Table 1 summarizes the times during which samples were collected from the 19th to 21st of March and 8th of April 2002. The corresponding mass concentration is shown in Fig. 7. At 0115 UTC March 20, the sky in Beijing turned yellow. The visibility was less than 200 m at 0300 UTC. The dust storm was observed from 0200 UTC March 19 to 0245 UTC March 20 with an average dust concentration of 0.39 mg m^{-3}. The severe dust storm occurred with the dust concentration increasing to 12.06 mg m^{-3} from 0250 to 0730 UTC March 20. This dust concentration is 40 times the daily average TSP Grade 2 Standard promulgated by the China Environment Protection Administration. After that, the dust concentration decreased quickly. The average dust concentrations during the period from 0740 to 1300 UTC March 20, from 1300 UTC March 20 to 0200 UTC March 21, and from 0200 UTC March 21 to 0200 UTC March 22 were 3.73, 3.07, and 1.52 mg m^{-3}, respectively. Thus, the dust storm impacted Beijing from 0300 UTC March 20 to 0200 UTC March 22. The simulated surface dust concentration at Beijing (40°N, 116°E) for different particle size groups from 0000 UTC March 19 to 0000 UTC March 22 is shown in Fig. 8. The simulated maximal total dust concentrations of 19th, 20th, and 21st of March were 6, 2, and 3 mg m^{-3}, respectively. The simulated dust concentration on March 20 is underestimated, but overestimated on the 19th of March 2002. Only for March 21, it is very similar to the observed amount.

Apart from analyzing the variation of surface concentration in Beijing, the surface concentration at 43°N, 114°E (near the Hunshandake sandy land) is also shown in Fig. 8. The dust concentration at the site is very dense with a maximal value of 100 mg m^{-3}. As

Table 1
Aerosol particle collections

Sample	Sample sampling period, UTC	Weather conditions
Mar. 19	0200 UTC March 19 to 0245 UTC March 20	Before dust period (clear)
Mar. 20a	0250 UTC March 20 to 0730 UTC March 20	Dust storm
Mar. 20b	0740 UTC March 20 to 1300 UTC March 20	Dust storm
Mar. 20c	1300 UTC March 20 to 0200 UTC March 21	Dust storm
Mar. 21	0200 UTC March 21 to 0200 UTC March 22	Dust storm
Mar. 22	0200 UTC March 22 to 0200 UTC March 23	After dust period (clear)
Apr. 08a	0100 UTC April 08 to 0400 UTC April 08	Dust storm
Apr. 08b	0400 UTC April 08 to 1130 UTC April 08	Dust storm

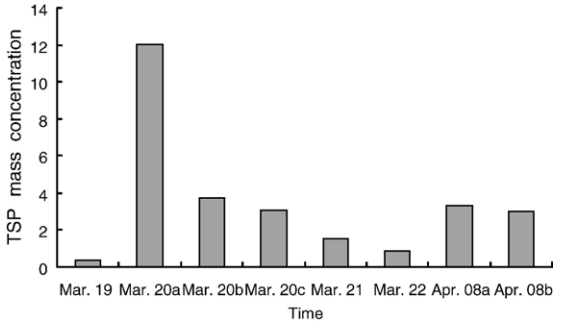

Fig. 7. Mass concentration of dust in the March and April 2002 (units: mg m^{-3}).

mentioned in Section 2, six particle size groups are used in the wind erosion and transportation scheme. The main airborne particles at the Beijing site originated from the 2 to 22 μm size range, whereas the dust emission of particle sizes less than 2 μm and greater than 22 μm was quite low (Fig. 8a–d). Otherwise, near the Hunshandake sandy land, airborne particles were composite of particle sizes $d \leq 22$ μm (Fig. 8g–l). Compared to the component of particles in Beijing, particle sizes of $d \leq 2$ μm are relatively important. The airborne particles near the Hunshandake sandy land are composite of particle sizes $d \leq 2$ μm (10%), $2 < d \leq 11$ μm (80%) and $11 < d \leq 22$ μm (10%), whereas at the Beijing site they are about $d \leq 2$ μm (2%), $2 < d < 11$ μm (49%) and $11 < d \leq 22$ μm (49%). You et al. (1991) pointed out that observed airborne particles mainly consist of particle sizes from 2 to 32 μm during the period of the severe dust storm in June 1986 in the vicinity of the Alashan Plateau. This observation is consistent with our simulation results.

4.2.2. Dust event during the 6th–9th of April 2002—case two

Similar to Fig. 5, dust concentration for the 6th–9th of April 2002 is compared with the observations in Fig. 9. Comparing the 19th–22nd of March with the 6th–9th of April 2002 events, quite similar features were observed in the evolution of the dust storms, but some differences also existed. First, the sandy lands in Inner Mongolia and the Gobi desert near the China–Mongolia border were the main dust source regions of this event. Second, smaller regions were affected during this event because the cyclone in this case was relatively weaker (Fig. 4).

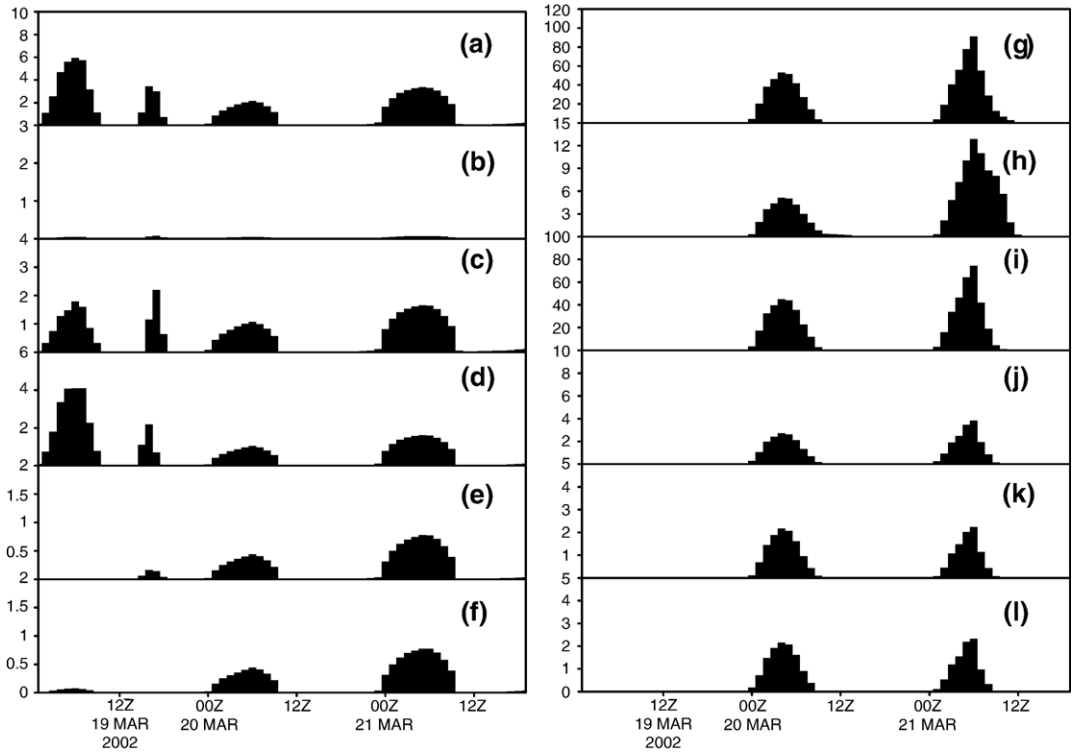

Fig. 8. Simulated surface dust concentration for different particle size groups from 0000 UTC March 19 to 0000 UTC March 22, 2002 at 40°N, 116°E (near Beijing, left panel) and 43°N, 114°E (near Hunshandake sandy land, right panel): (a and g) total; (b and h) $d \leq 2$ μm; (c and i) $2 < d \leq 11$ μm; (d and j) $11 < d \leq 22$ μm (units: mg m^{-3}); (e and k) dust deposition (units: mg m^{-2} s^{-1}) and (f and l) dust flux (units: mg m^{-2} s^{-1}).

Severe dust activities appeared over southern Mongolia and Inner Mongolia at 0300 UTC April 6, and the dust-affected area extended widely across Inner Mongolia at 0600 UTC April 6 (Fig. 9a, b). On the 7th of April, the region experienced severe dust storms extending from southeast Mongolia to the northern part of Hebei province, and at the same time, dust-in-suspension was widely observed over the eastern part of northeast China, but this large observed area of dust-in-suspension was not simulated successfully by the modeling system (Fig. 9c, d). On the 8th of April, the simulated dust-affected area was much smaller than in the previous day, while severe dust storm was also observed at only a few stations. The dust concentration

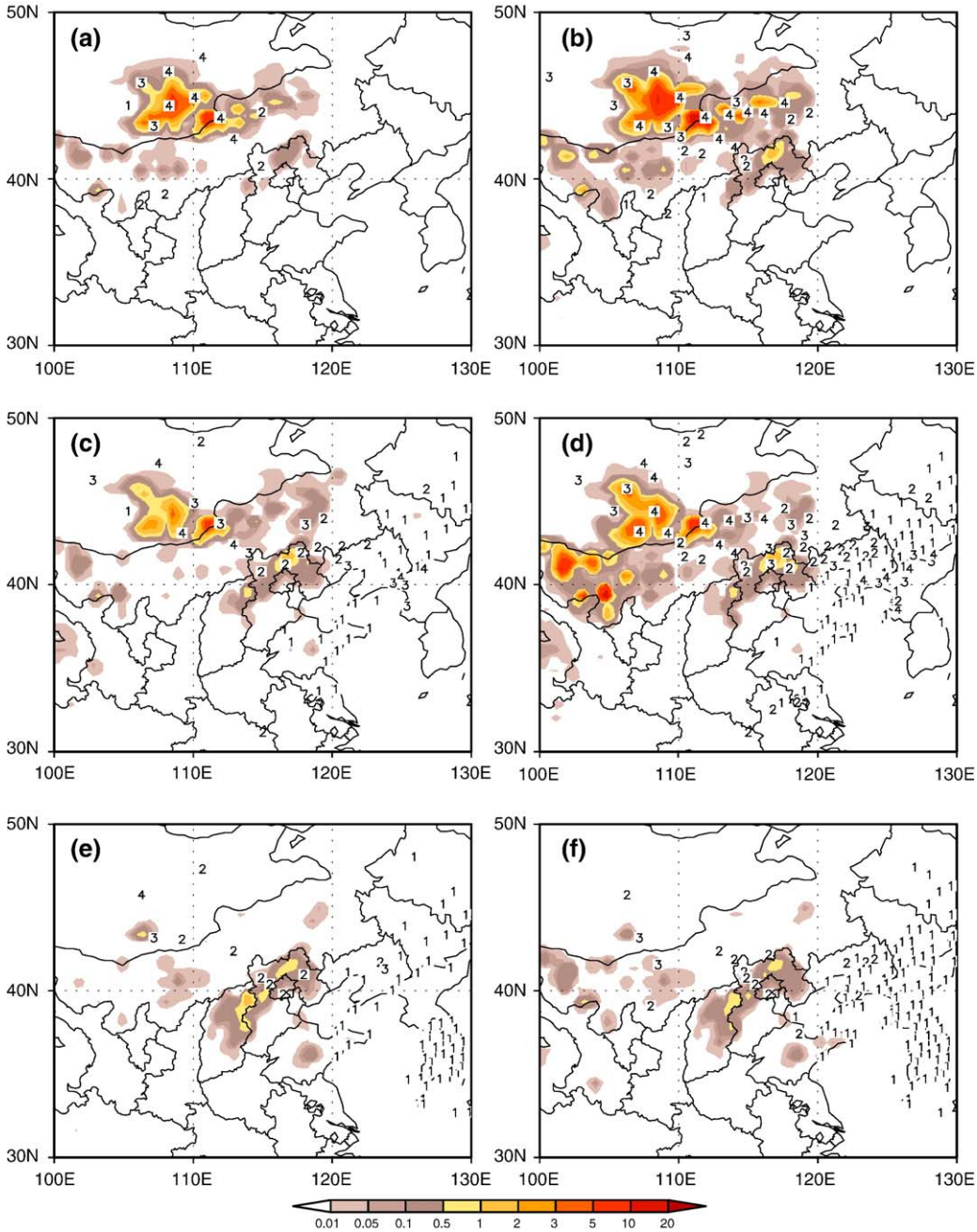

Fig. 9. As Fig. 5, but for (a) 0300 UTC April 6; (b) 0600 UTC April 6; (c) 0300 UTC April 7; (d) 0600 UTC April 7; (e) 0300 UTC April 8; and (f) 0600 UTC April 8, 2002.

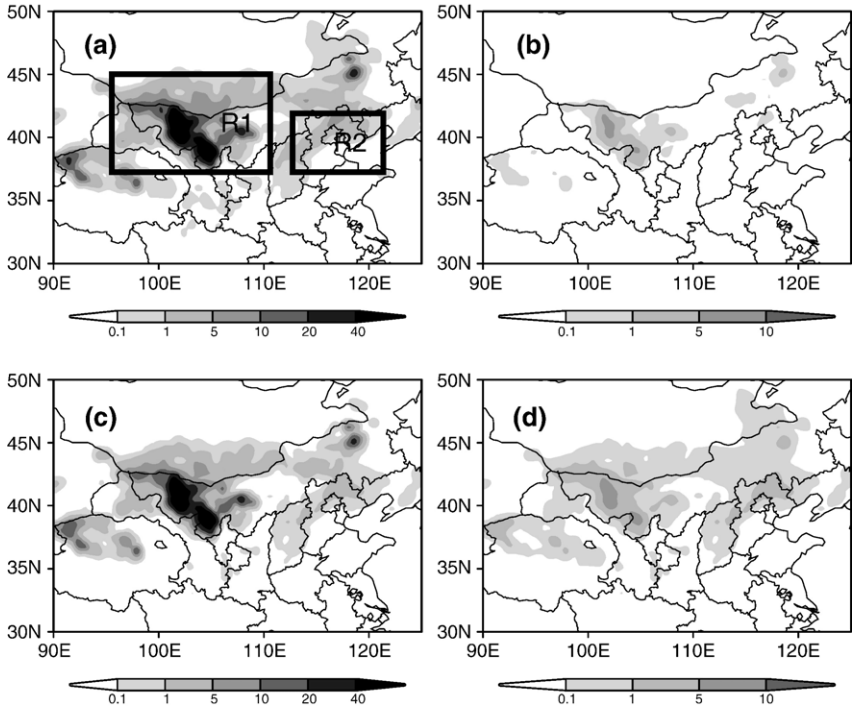

Fig. 10. Simulated average dust flux of 0000 UTC March 19–0000 UTC March 22, 2002 (units: mg m^{-2} s^{-1}). The dust source regions are marked R1 and R2. (a) $d \leq 22$ μm; (b) $d \leq 2$ μm; (c) $2 < d \leq 11$ μm; and (d) $11 < d \leq 22$ μm.

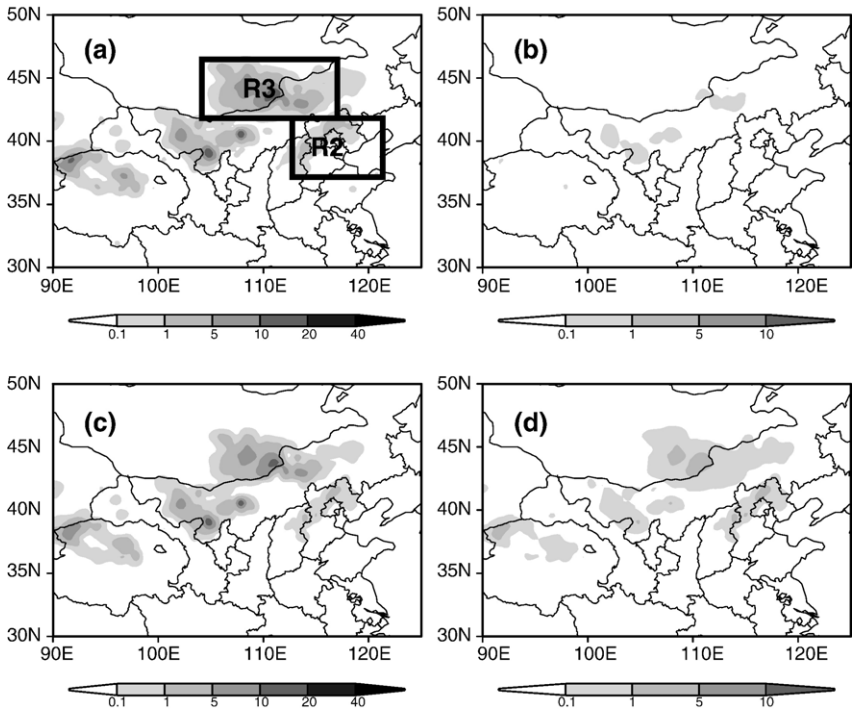

Fig. 11. As Fig. 10, but for 0000 UTC 6 April–0000 UTC 9 April 2002. The dust source regions are marked R2 and R3.

in Beijing is about 3 mg m^{-3} on the 8th of April (Fig. 7), whereas the simulation is only 1 mg m^{-3}, smaller than that in observation. During the period of this event, two deficiencies in the simulation exist: (1) the simulated strong dust emission of sandy lands over western Inner Mongolia is not consistent with observations (Fig. 9d); and (2) the observed dust-in-suspension over northeast China and the Korean Peninsula is not simulated successfully.

However, some common deficiencies exist in the simulation results of the two events, for example, the dust activities in Mongolia and Liaoning province are not correctly simulated probably because of the poor land surface data for those regions in use in the present study. The dust emission on sandy lands located in central Inner Mongolia is too strong compared to the observations, for instance, a high concentration is simulated despite that no observed dust event is recorded there. The modeling system exhibits another important weakness that the simulated dust events are weaker during the night compared to observations. This may be caused by a coarser description of the diurnal variation of the PBL. Despite some differences between the simulation and observation, generally speaking, the modeling system is still skilful in simulating the weather system, such as in the propagation and development of Mongolian cyclones, the dust emission, transportation and deposition over the Gobi desert, sandy lands in southern Mongolia, and the northern part of China.

4.3. Dust sources

On the basis of the comparisons presented above, the integrated modeling system has the capacity to simulate the main features during dust storm events over northern China and Mongolia. In this section, the hourly simulations of two dust events are used to analyze the dust sources, their variation and components.

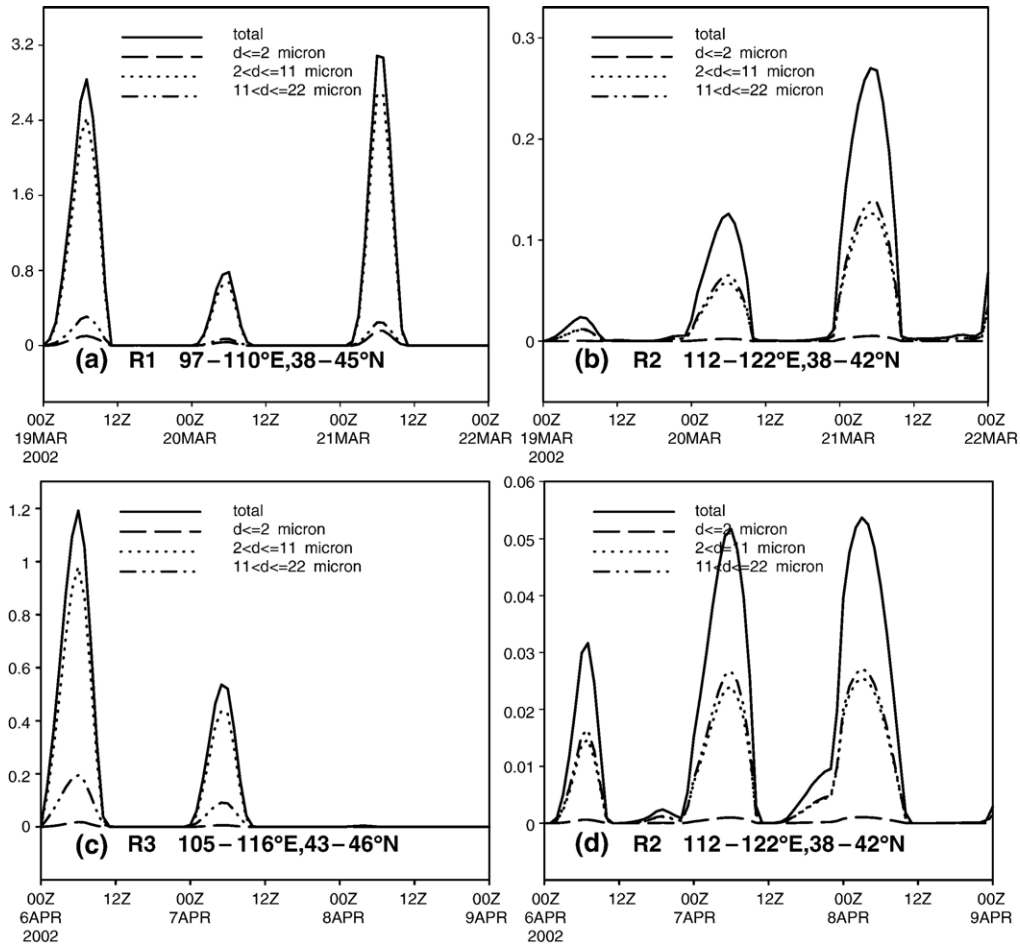

Fig. 12. Average simulated dust flux (units: mg m^{-2} s^{-1}) of southern Mongolia, western Inner Mongolia and North China for (a and b) 0000 UTC March 19–0000 UTC March 22, 2002; and (c and d) 0000 UTC April 6–0000 UTC April 9, 2002.

Since particle sizes of $d>22$ μm are not generally emitted, the average dust emission for different particle size groups ($d\leq 22$ μm) are displayed for the 19th–22nd of March in Fig. 10 and for the 6th–9th of April 2002 in Fig. 11. The most important dust sources for the two events are somewhat different. The sandy lands over southern Mongolia and western Inner Mongolia (marked by R1 in Fig. 10a) are the main sources of the first event. In contrast, the dust originates from the Mongolia–Inner Mongolia border in the second case (marked by R3 in Fig. 11a). The area and intensity of dust emission in the first case is wider and higher than those in the second case (Figs. 10a and 11a). For particle sizes $d\leq 2$ μm, significant dust flux over western Inner Mongolia in case one is simulated well, but it is quite weak in case two. The main dust source of particle sizes of $2<d\leq 11$ μm is Gansu, western Qinghai and western Inner Mongolia (Figs. 10c and 11c). The contribution of particle sizes of $11<d\leq 22$ μm to total dust emission is not as important as the particle size range $2<d\leq 11$ μm, but its influence cannot be neglected. According to the above analysis, except for the Gobi desert over southern Mongolia, the dust sources for the two cases are the Badain Jaran Desert, Tengger Desert and Hunshandake sandy land in Inner Mongolia.

In the wind erosion model, the dust emission rate is highly related to soil type, soil moisture and wind speed. For different regions, the dust emission rate of each particle size group is significantly different according to the above analysis, for instance, between the western and central parts of Inner Mongolia. To understand exactly the particle size components for the different regions, three regions are selected. Region 1 is defined as 38–45°N, 97–110°E (R1 in Fig. 10a) including the sandy lands in western Inner Mongolia and the Gobi desert in southern Mongolia, whereas Region 2 is defined by 38–42°N, 112–122°E (R2 in Figs. 10a and 11a) including Beijing and its surrounding area. Region 3 is defined by 43–46°N, 105–116°E (marked by R3 in Fig. 11a) and is only used in case two. The average dust flux for these regions is given in Fig. 12. The daily variation, with a maximal value occurring at 0600 UTC (14 LST) is significantly revealed, and this is consistent with the observation (Fig. 3). For the two cases, the dust emission rates of particle sizes $2<d\leq 11$ μm and $11<d\leq 22$ μm are almost equivalent over Region 2 (Fig. 12b, d), but particle sizes of $2<d\leq 11$ μm

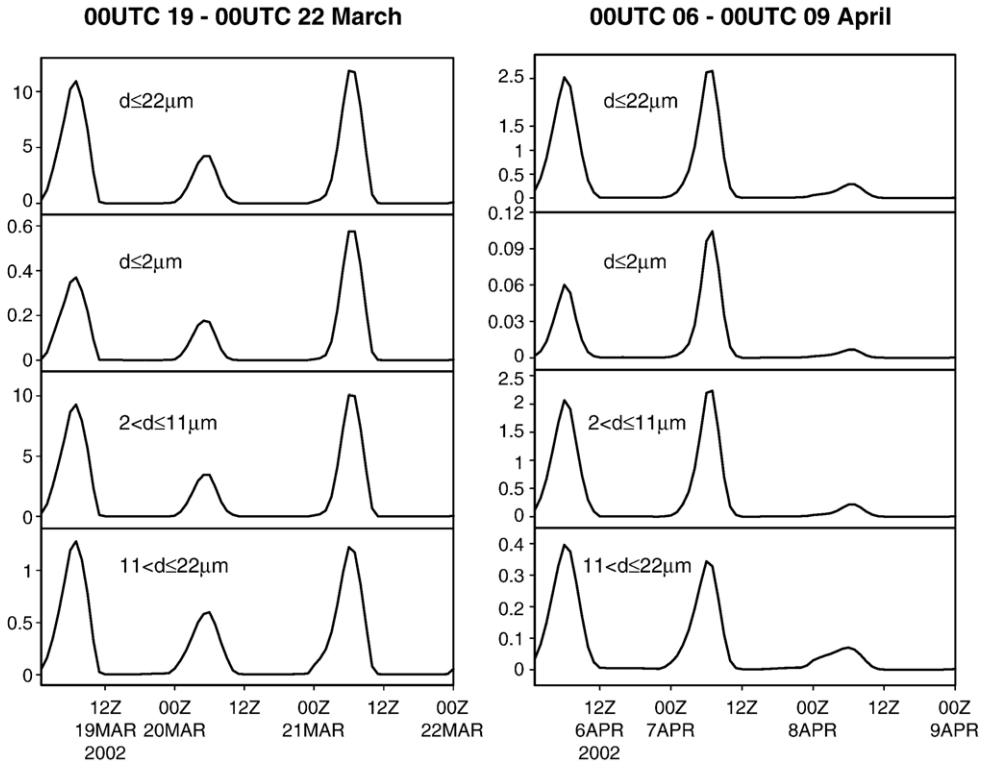

Fig. 13. Hourly dust flux in Mt h^{-1} for the entire simulation domain for different particle size groups during 0000 UTC March 19–0000 UTC March 22, 2002 (left panel) and 0000 UTC April 6–0000 UTC April 9, 2002 (right panel).

comprise 90% of the total dust emission for Regions 1 and 3 (Fig. 12a, c). The dust emission rates of particle sizes $d \leq 2$ μm for the three regions are very weak, and thus this range is not the main source of the dust storm.

The spatial distribution and temporal variation of the dust emission rate for the two dust events have already been discussed, respectively. The total amount of dust emission from the entire simulation domain, centered at 40°N, 115°E with a range of 6750×5400 km, can be calculated according to the following formula:

$$\mathrm{FT\_DOM(t)} = \sum_{i=1,j=1}^{I,J} Ft(i,j,t)\Delta x \Delta y$$

where Δx and Δy are horizontal grid distance, and I, J are the total number of grids in the x and y directions. The values of FT_DOM for the three particle size groups, $d \leq 2$ μm, $2 < d \leq 11$ μm, and $11 < d \leq 22$ μm, and the total are given in Fig. 13. During the two severe dust storms, the maximum values of FT_DOM were 12 and 2.7 Mt h^{-1}, respectively. The maximal FT_DOM for case one is about 4–5 times as much as that of case two. More than 80% of the total dust emission rate was from particle size group $2 < d \leq 11$ μm. Compared to the total dust emission rate, particle sizes $d = 2$μm can be neglected, whereas the range $11 < d \leq 22$ μm is relatively important.

5. Conclusions and discussions

An integrated dust storm numerical modeling system for the East Asia area has been developed by coupling a physically based dust emission model, a dust transportation model and a non-hydrostatic meso-scale model (MM5) with a geographic information database. This system can be used to predict dust emission rates and dust concentration associated with individual dust storm events. Numerical simulations using this system have been conducted and the preliminary results are presented in this paper.

The characteristics of East Asian dust storms are analyzed. It is found that the intensities of the dust storms have obvious diurnal variations with severe dust storms occurring more frequently in the afternoon and weak dust storms in the morning. The diurnal variation of light dust storms is weaker than that of severe dust storms. Two severe dust events occurred during the 19th–22nd of March and the 6th–9th of April. The strong northwesterly wind in the cold air region behind the cold front associated with Mongolian cyclones resulted in dust emission and transportation.

The integrated system is employed to simulate the dust storm events of the 19th–22nd of March and the 6th–8th of April 2002. In comparison with synoptic records and satellite images, the dust events are found to be well predicted in terms of spatial and temporal evolution. It is shown that the integrated system is capable of predicting dust source and dust transportation although some deficiencies in the modeling system need to be improved in the future.

The hourly simulation results are used to analyze the dust sources of these events. The dust sources of the two events are the Gobi desert in southern Mongolia, the Badain Jaran Desert, Tengger Desert and Hunshandake sandy land. However, the dominant mode of dust particles is in the 2–11 μm size range over the western part of Inner Mongolia and Mongolia and in the 2–22 μm size range over Beijing and its surrounding area. The maximal dust emission for the entire simulation domain reaches 12 and 2.7 Mt h^{-1} for the two events, respectively. Compared to the total dust emission rate, the dust emission rate of particle sizes $2 < d \leq 11$ μm is the most important dust source, and the $11 < d < 22$ μm size range is also relatively important. The other particle size groups can be neglected in the total dust emission rate.

This study has some limiting factors that can be improved in the future: (1) no initiation of dust concentration data is available; (2) wet deposition is not processed; (3) the geographic information system (GIS) data used in this work has uncertainties in quantities such as the soil type in Mongolia and the soil particle size distribution.

Acknowledgements

This study is supported by the Ministry of Finance of China Project Y0101 “Monitoring and Prediction of Soil Moisture and Dust Storms in Northwest China”. The authors are grateful to Dr. Y. Shao for providing us with the dust emission and dust transportation schemes and for giving valuable suggestions. The satellite monitoring images and the GIS database are provided by the National Satellite Meteorological Center, China Meteorological Administration and the Institute of Geographical Sciences and Natural Resources, Chinese Academy of Sciences, respectively.

References

Chatenet, B., Marticorena, B., Gomes, L., Bergametti, G., 1996. Assessing the microped size distributions of desert soils erodible by wind. Sedimentology 43, 901–911.

Chen, F., Dudhia, J., 2001a. Coupling and advanced land surface-hydrology model with the Penn State-NCAR MM5 modeling system: Part II. Preliminary model validation. Mon. Weather Rev. 129, 587–604.

Chen, F., Dudhia, J., 2001b. Coupling an advanced land surface-hydrology model with the Penn State-NCAR MM5 modeling system. Part I: model implementation and sensitivity. Mon. Weather Rev. 129, 569–585.

Cheng, L.S., Ma, Y., 1996. The developing structure of a black storm and its numerical experiment of different model resolution. Quart. J. Appl. Meteorol. 7, 386–395 (in Chinese, with English Abstr.).

Grell, G., Dudhia, J., Stauffer, D., 1994. A description of the Fifth-generation Penn State/NCAR mesoscale model (MM5). NCAR Tech. Note. NCAR/TN-398+STR, 117pp.

Hong, S.-Y., Pan, H.-L., 1996. Nonlocal boundary layer vertical diffusion in a medium range forecast model. Mon. Weather Rev. 124, 2322–2339.

Huang, M.Y., Wang, Z., 1998. A model for long-range transport of yellow-sand in East Asia. Chin. J. Atmos. Sci. 22, 905–912 (in Chinese, with English Abstr).

Li, X.S., Zhou, J.Q., Li, Z., Fang, X.M., He, Z.S., Parungo, F., 1998. A numerical simulation of "5.5" super-duststorm in northern China. Adv. Atmos. Sci. 15, 63–73.

Liu, C.T., Cheng, L.S., 1997. Parameterization of the formation and transportation for sand-dust of the black storm and mesoscale numerical experiments. ACTA Meteorol. Sin. 55 (6), 726–738 (in Chinese, with English Abstr).

Liu, Y., Ren, L.X., Zhou, L.Y., Zhou, M.Y., Gao, Y., 1998. Numerical analyses of dust storm and dust transportation. Chin. J. Atmos. Sci. 22, 905–912 (in Chinese, with English Abstr).

Lu, H., Shao, Y.P., 1999. A new model for dust emission by saltation bombardment. J. Geophys. Res. 104, 16827–16841.

Lu, H., Shao, Y., 2001. Toward quantitative prediction of dust storms: an integrated wind erosion modeling system and its applications. Environ. Model. Softw. 16, 233–249.

Marticorena, B., Bergametti, G., 1995. Modeling the atmospheric dust cycle: Part I. Design of a soil-derived dust emission scheme. J. Geophys. Res. 100, 16415–16430.

Marticorena, B., Bergametti, G., Aumont, B., Callot, Y., N'Doume, C., Legrand, M., 1997. Modeling the atmospheric dust cycle. Part II. Simulation of Saharan dust sources. J. Geophys. Res. 102, 4387–4404.

Raupach, M.R., Lu, H., 2004. Representation of land-surface processes in aeolian transport models. Environ. Model. Softw. 19, 93–112.

Shao, Y., 2000. Physics and Modelling of Wind Erosion. Kluwer Academic Publishers, Netherlands, pp. 139–142.

Shao, Y., 2001. A model for mineral dust emission. J. Geophys. Res. 106, 20239–20254.

Shao, Y., 2004. Simplification of a dust emission scheme and comparison with data. J. Geophys. Res. 109, D10202. doi:10.1029/2003JD004372.

Shao, Y., Lu, H., 2000. A simple expression for wind erosion threshold friction velocity. J. Geophys. Res. 105, 22,437–22,444.

Shao, Y., Raupach, M.R., Leys, J.F., 1996. A model for predicting Aeolian sand drift and dust entrainment on scales from paddock to region. Aust. J. Soil Res. 34, 309–342.

Wang, Z.F., Ueda, H., Huang, M.Y., 2000. A deflation module for use in modeling long-range transport of yellow sand over East Asia. J. Geophys. Res. 105, 26947–26959.

Ye, D.Z., Chou, J.F., Liu, J.Y., Zhang, Z.X., Wang, Y.M., Zhou, Z.J., Ju, H.B., Huang, H.Q., 2000. Causes of sand-stormy weather in northern China and control measures. Acta Geogr. Sin. 55, 513–521.

You, L.G., Ma, P.M., Chen, J.H., Li, K., 1991. A case study of the aerosol characteristics in the lower troposphere during a dust storm event. Quart. J. Appl. Meteorol. 2, 13–21 (in Chinese, with English Abstr).

Zender, C.S., Bian, H., Newman, D., 2003. Mineral Dust Entrainment and Deposition (DEAD) model: description and 1990s dust climatology. J. Geophys. Res. 108 (D14), 4416. doi:10.1029/2002JD002775.

Zhang, X.Y., 2001. Source distributions, emission, transport, deposition of Asian dust and Loess accumulation. Quat. Sci. 21, 29–38.

Zhang, R.J., Han, Z.W., Wang, M.X., Zhang, X.Y., 2002. Dust storm weather in China: new characteristics and origins. Quat. Sci. 22, 374–380 (in Chinese, with English Abstr).

Zhang, S.H., Peng, G.B., Huang, M., 2004. The feature extraction and data fusion of regional soil textures based on GIS techniques. Clim. Environ. Res. 9 (1), 65–79 (in Chinese, with English Abstr).

Zhang, R.J., Arimoto, R., An, J.L., Yabuki, S., Sun, J.H., 2005. Ground observations of a strong dust storm in Beijing in March 2002. J. Geophys. Res. 110 (D18), D18S06. doi:10.1029/2004JD004589.

Zhao, L.N., Zhao, S.X., 2006. Diagnosis and simulation of a rapidly developing cyclone related to a severe dust storm in East Asia. Glob. Planet. Change. 52, 105–120. doi:10.1016/j.gloplacha.2006.02.003 (this issue).

Zhou, Z.J., 2001. Blowing sand and sand storm in China in recent 45 years. Quat. Sci. 21, 9–17.

Zhuang, G.S., Guo, J.H., Yuan, H., Zhao, C.Y., 2001. The compositions, sources, and size distribution of the dust storm from China in spring of 2000 and its impact on the global environment. Chin. Sci. Bull. 46 (1), 895–900 (in Chinese, with English Abstr.).